

Electronic Supplementary Information

Ultrathin Ti-doped WO₃ Nanosheets Realizing Selective Photoreduction of CO₂ to CH₃OH

Peiquan Ling,^{‡a} Juncheng Zhu,^{‡a} Zhiqiang Wang,^a Jun Hu,^a Junfa Zhu,^a Wensheng Yan,^a Yongfu Sun^{*a,b} and Yi Xie^{*a,b}

^aHefei National Research Center for Physical Sciences at the Microscale, National Synchrotron Radiation Laboratory, University of Science and Technology of China, Hefei 230026, China. Email: yfsun@ustc.edu.cn; yxie@ustc.edu.cn

^bInstitute of Energy, Hefei Comprehensive National Science Center, Hefei 230031, China.

[‡]These authors contributed equally to this work

Experiment section

Synthesis of the Ti-WO₃ nanosheets. In a typical procedure, 0.5 g of Na₂WO₄·2H₂O was dissolved in 20 mL of deionized water in a three-necked round-bottom flask equipped with reflux condenser under stirring. The mixture was heated to 70 °C, followed by addition of 0.306 g of C₁₇H₃₅COONa. After 20 min of stirring, 20 mL of concentrated sulfuric acid was added drop by drop, while the inner temperature was kept below 100 °C. Then, a certain amount (0.036 g) of Ti(SO₄)₂ were added to the mixture. Subsequently, the mixture was heated at 160 °C for 5.0 h using an oil bath. After cooled to room temperature, the reaction mixture was carefully diluted by lots of deionized water, and the solid was collected through centrifugation. The obtained sample was washed with deionized water and ethanol for several times. The product was dried in a vacuum at 60 °C overnight, then calcined in air at a heating rate of 10 °C/min for 1 h at 350 °C. The obtained powders were collected for further characterization. The amount of Ti dopants in Ti-WO₃ nanosheets could be adjusted by altering the amount of Ti(SO₄)₂ addition.

Synthesis of the WO₃ nanosheets. In a typical procedure, 0.5 g of Na₂WO₄·2H₂O was dissolved in 20 mL of deionized water in a three-necked round-bottom flask equipped with reflux condenser under stirring. The mixture was heated to 70 °C, followed by addition of 0.306 g of C₁₇H₃₅COONa. After 20 min of stirring, 20 mL of concentrated sulfuric acid was added drop by drop while the inner temperature was kept below 100 °C. Then, the mixture was heated at 160 °C for 5.0 h using an oil bath. After cooled to room temperature, the reaction mixture was carefully diluted by lots of deionized water, and the solid was collected through centrifugation. The obtained sample was washed with deionized water and ethanol for several times. The product was dried in a vacuum at 60 °C overnight, then calcined in air at a heating rate of 10 °C/min for 1 h at 350 °C. The obtained powders were collected for further characterization.

Characterization. TEM images were obtained using a JEOL-2010 TEM system. The HRTEM and the corresponding energy dispersive spectroscopy mapping analyses were performed on a JEOL JEM-ARM200F TEM/STEM with a spherical aberration corrector. XRD patterns were recorded using a Philips X'Pert Pro Super diffractometer with Cu K α radiation ($\lambda = 1.54178\text{\AA}$). AFM measurements were performed using a Veeco DI Nano-scope MultiMode V system. UV-vis diffuse reflectance spectroscopy was performed on a UV-vis-NIR spectrophotometer (Perkin Elmer Lambda 950). Raman spectra were detected by LabRamHR Evolution System, in which the excitation wavelength was at 532 nm. PL spectra were acquired on a luminescence spectrometer (Jobin Yvon Fluorolog 3-TAU, Jobin Yvon Instruments), in which the excitation pulse was generated by a 450W Xe lamp. Time-resolved PL (TRPL) spectra were measured on HORIBA DeltaFlex TCSPC system. *In situ* FTIR spectra were obtained by using a Thermo Scientific Nicolet iS50. Synchrotron-radiation X-ray absorption near-edge spectroscopy (XANES) was measured at the National Synchrotron Radiation Laboratory (NSRL), China. Ultraviolet photoelectron spectroscopy was performed at the Catalysis and Surface Science Endstation at the BL11U beamline of the National Synchrotron Radiation Laboratory (NSRL). The work function (WF) was determined by the difference between the photon energy and the binding energy of the secondary cutoff edge. To be exact, $E_B = h\nu - (E_K + 4.3 - 5.0)$ and $W_F = h\nu - (E_{\text{cutoff}} - E_F)$ (E_B , binding energy; $h\nu$, photon energy; E_K , kinetic energy; E_{cutoff} , secondary cutoff edge; E_F , Fermi level; photon energy of 40.0 eV).

and a sample bias of -5V applied to observe the secondary electron cutoff). Synchrotron-radiation vacuum ultraviolet photoionization mass spectrometry was executed at the combustion endstation of the BL03U beamline of the National Synchrotron Radiation Laboratory (NSRL). Quasi *in situ* XPS and XANES spectra were acquired at the Catalysis and Surface Science Endstation at the BL11U beamline of the National Synchrotron Radiation Laboratory (NSRL). XPS spectra were acquired on an ESCALAB MKII system with Al K α ($h\nu = 1,486.6$ eV) as the excitation source. The binding energies obtained in the XPS spectral analysis were corrected for specimen charging by referencing C 1s to 284.8 eV.

Photocatalytic CO₂ reduction measurement. In the typical CO₂ photocatalytic reduction process, 5 mg of the as-synthesized WO₃ powders was initially dispersed in deionized water and then the dispersions were dripped onto the quartz glass dish. After heating at 65 °C for 0.5 h, the WO₃-based thin film was prepared. Then, the quartz glass dish was put in the reaction cell with 10 mL of deionized water on the bottom, where the volume of the reaction cell was approximately 200 mL. Hence, the reaction cell was vacuum-treated for several times, which was then pumped by high-purity CO₂ to reach an atmospheric pressure. The temperature of the reaction cell was controlled at 25 °C by recirculating cooling water system during irradiation. The light source for the photocatalysis was a CEL-HXF300 Xe lamp (Beijing China Education Au-light Co., Ltd.) with a standard AM 1.5G filter, in which the outputting light density was about 100 mW/cm². During the light irradiation, the gas products were qualitatively analyzed by Agilent GC-7890B gas chromatograph by identifying the chromatographic peaks. The liquid products were quantified by nuclear magnetic resonance (Bruker AVANCE AV III 400) spectroscopy, in which dimethyl sulfoxide (Sigma, 99.99%) was added as an internal standard. When a new catalytic cycle began, the catalyst was washed by distilled water in order to remove surface-adsorbed reactants.

***In situ* FTIR measurements.** *In situ* FTIR spectra were obtained by using a Thermo Scientific Nicolet iS50, equipped with a MCT detector cooled by liquid nitrogen and a commercial reaction chamber from Harrick Scientific. After degassed at 120 °C in N₂ atmosphere for 20 min, the gas flow was switched to high-purity CO₂ for adsorption. The background spectrum was collected after 20 minutes of adsorption in high-purity CO₂. Each spectrum was recorded by averaging 64 scans at 4 cm⁻¹ spectral resolution.

Quasi *in situ* XPS measurements. Quasi *in situ* XPS measurements were performed at the photoemission end-station at beamline BL11U in the National Synchrotron Radiation Laboratory (NSRL) in Hefei, China. The end-station is composed of three chambers—an analysis chamber, a preparation chamber, a load-lock chamber. The analysis chamber, with a base pressure of < 10⁻¹¹ torr, is connected to the beamline with a VG Scienta R4000 electron energy analyser. In the current work, the sample was treated with 10⁻⁵ mbar of CO₂ in the preparation chamber. After the sample treatment, the preparation chamber can be pumped with pressure down to < 10⁻⁹ mbar for sample transfer. Then, the sample was transferred to the analysis chamber for XPS measurement without exposing it to air.

Quasi *in situ* XANES measurements. Quasi *in situ* XANES measurements were performed at the photoemission end-station at beamline BL11U in the National Synchrotron Radiation Laboratory

(NSRL) in Hefei, China. The end-station is composed of three chambers—an analysis chamber, a preparation chamber, a load-lock chamber. The analysis chamber, with a base pressure of $< 10^{-11}$ torr, is connected to the beamline with a VG Scienta R4000 electron energy analyser. In the current work, the sample was treated with 10^{-5} mbar of CO_2 in the preparation chamber. After the sample treatment, the preparation chamber can be pumped with pressure down to $< 10^{-9}$ mbar for sample transfer. Then, the sample was transferred to the analysis chamber for XANES measurement without exposing it to air.

DFT calculation details. The first-principles calculations were performed with the Vienna ab initio simulation package^{1, 2}. The interaction between ions and valence electrons was described using projector augmented wave (PAW) potentials, and the exchange-correlation between electrons was treated through using the generalized gradient approximation (GGA) in the Perdew-Burke-Ernzerhof (PBE) form³. To achieve the accurate density of the electronic states, the plane wave cutoff energy was 420 eV, a Gamma-center $5 \times 5 \times 1$ for sheet K point mesh were used. The ionic relaxations for all structures in the calculations were carried out under the conventional energy (10^{-3} eV) and force (0.02 eV/Å) convergence criteria. The WO_3 slab along the [0 1 0] projection was used to mimic the as-prepared nanosheets, where a 1.5 nm vacuum layer was added to avoid interactions.

Gibbs free energies for each gaseous and adsorbed species were calculated at 298.15 K, according to the expression:

$$G = E_{\text{DFT}} + E_{\text{ZPE}} - TS$$

$$E_{\text{ZPE}} = \sum_i 1/2 h\nu_i$$

$$\Theta_i = h\nu_i / k$$

$$S = \sum_i R [\ln (1 - e^{-\Theta_i/T})^{-1} + \Theta_i/T (e^{\Theta_i/T} - 1)^{-1}]$$

where E_{DFT} is the electronic energy calculated for specified geometrical structures, E_{ZPE} is the zero-point energy, S is the entropy, h is the Planck constant, ν is the computed vibrational frequencies, Θ is the characteristic temperature of vibration, k is the Boltzmann constant, and R is the molar gas constant. For adsorbates, all 3N degrees of freedom were treated as frustrated harmonic vibrations with negligible contributions from the catalysts' surfaces. We treated the charge of the system refer to the widely-recognized computational hydrogen electrode (CHE) mode,⁴ in which each reaction step was regarded as a simultaneous transfer of the proton-electron pair as a function of the applied potential. Thus, free energy changes relative to an initial state of gaseous CO_2 free above an empty surface can be represented by

$$\Delta G [\text{COOH}^*] = G [\text{COOH}^*] + 7 \times G [\text{H}^+ + \text{e}^-] - (G [*] + G [\text{CO}_2] + 8 \times G [\text{H}^+ + \text{e}^-])$$

$$\Delta G [\text{CO}^*] = G [\text{CO}^*] + G [\text{H}_2\text{O}] + 5 \times G [\text{H}^+ + \text{e}^-] - (G [*] + G [\text{CO}_2] + 6 \times G [\text{H}^+ + \text{e}^-])$$

$$\Delta G [* + \text{CO}] = G [*] + G [\text{CO}] + G [\text{H}_2\text{O}] + 4 \times G [\text{H}^+ + \text{e}^-] - (G [*] + G [\text{CO}_2] + 6 \times G [\text{H}^+ + \text{e}^-])$$

$$\Delta G [\text{CHO}^*] = G [\text{CHO}^*] + G [\text{H}_2\text{O}] + 3 \times G [\text{H}^+ + \text{e}^-] - (G [*] + G [\text{CO}_2] + 6 \times G [\text{H}^+ + \text{e}^-])$$

$$\Delta G [\text{CH}_2\text{O}^*] = G [\text{CH}_2\text{O}^*] + G [\text{H}_2\text{O}] + 2 \times G [\text{H}^+ + \text{e}^-] - (G [*] + G [\text{CO}_2] + 6 \times G [\text{H}^+ + \text{e}^-])$$

$$\Delta G [\text{CH}_3\text{O}^*] = G [\text{CH}_3\text{O}^*] + G [\text{H}_2\text{O}] + G [\text{H}^+ + \text{e}^-] - (G [*] + G [\text{CO}_2] + 6 \times G [\text{H}^+ + \text{e}^-])$$

$$\Delta G [\text{CH}_3\text{OH}^*] = G [\text{CH}_3\text{OH}^*] + G [\text{H}_2\text{O}] - (G [*] + G [\text{CO}_2] + 6 \times G [\text{H}^+ + \text{e}^-])$$

$$\Delta G [* + \text{CH}_3\text{OH}] = G [\text{CH}_3\text{OH}] + G [*] + G [\text{H}_2\text{O}] - (G [*] + G [\text{CO}_2] + 6 \times G [\text{H}^+ + \text{e}^-])$$

$$G [\text{H}^+ + \text{e}^-] = 1/2G [\text{H}_2] - eU$$

where * is the substrate, U is the applied overpotential and e is the elementary charge. In this study, $U = 0$ V versus reversible hydrogen electrode.

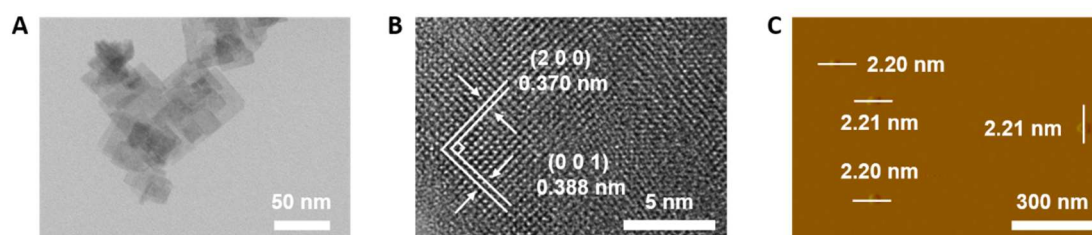


Figure S1. (A) TEM image of the WO_3 nanosheets. (B) HRTEM image of the WO_3 nanosheets, showing the 0.367 nm and 0.382 nm interplanar distances that matched well with the d_{200} and d_{001} planes, respectively. (C) AFM image of the WO_3 nanosheets.

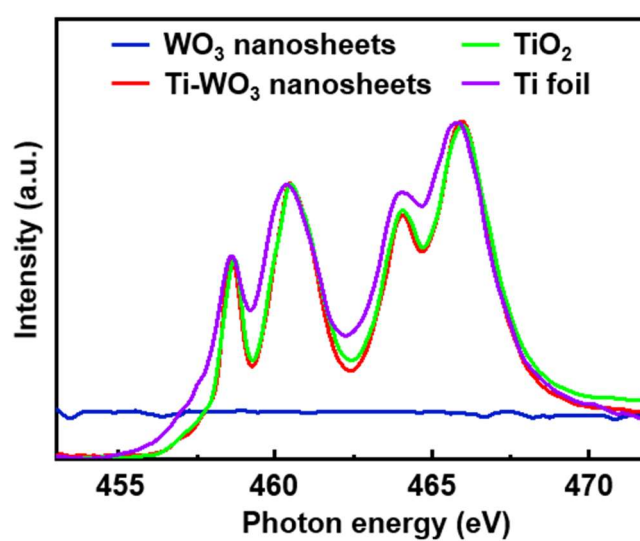


Figure S2. Synchrotron-radiation XANES spectra of the Ti-WO_3 nanosheets, the WO_3 nanosheets, TiO_2 reference and Ti foil reference.

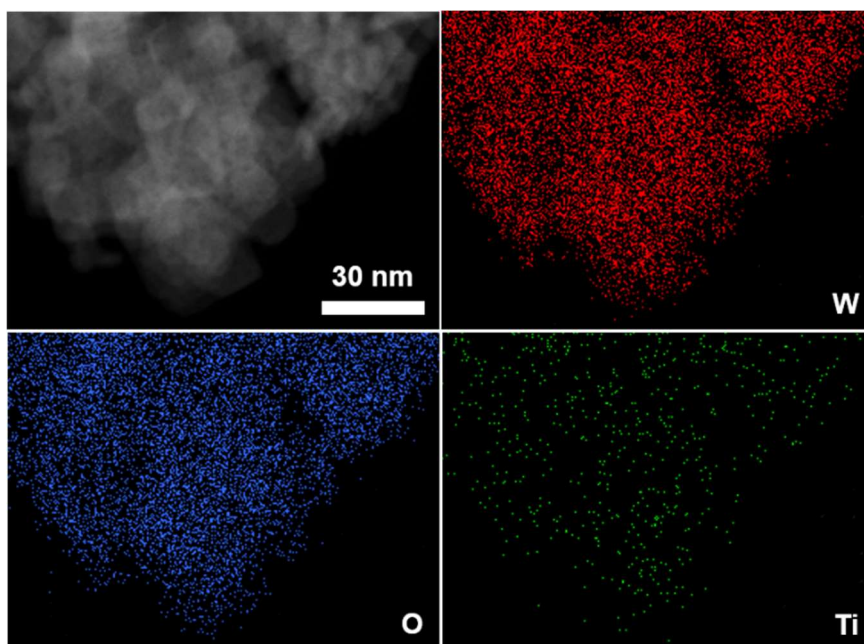


Figure S3. Annular dark-field TEM image and the corresponding element mappings of the Ti-WO₃ nanosheets.

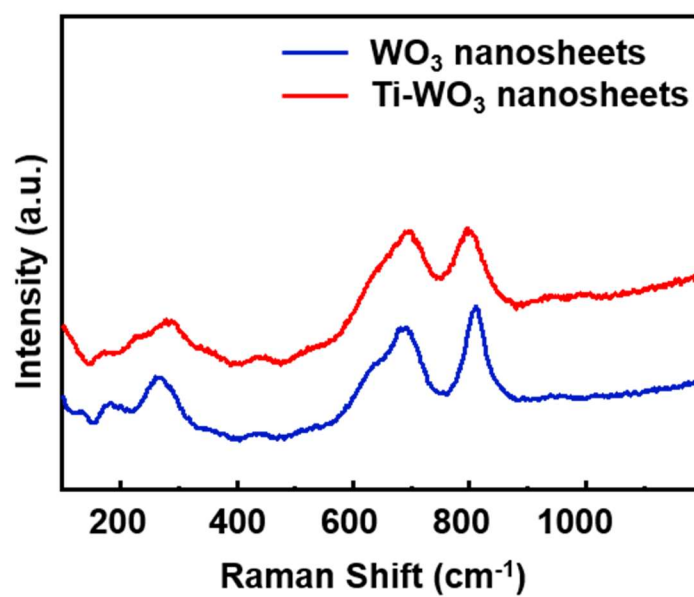


Figure S4. Raman spectra of the Ti-WO₃ nanosheets and the WO₃ nanosheets.

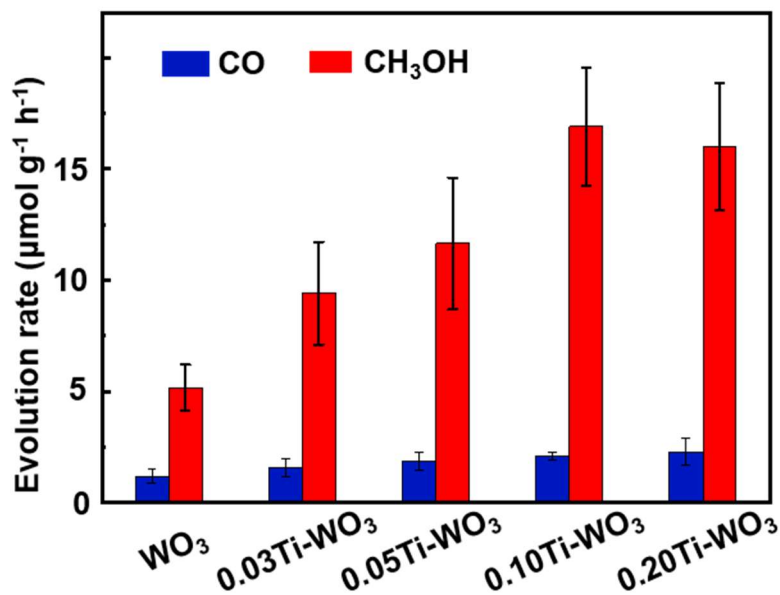


Figure S5. Products of photocatalytic CO₂ reduction for WO₃ nanosheets with different amounts of Ti doping. The error bars represent the standard deviations of three independent measurements.

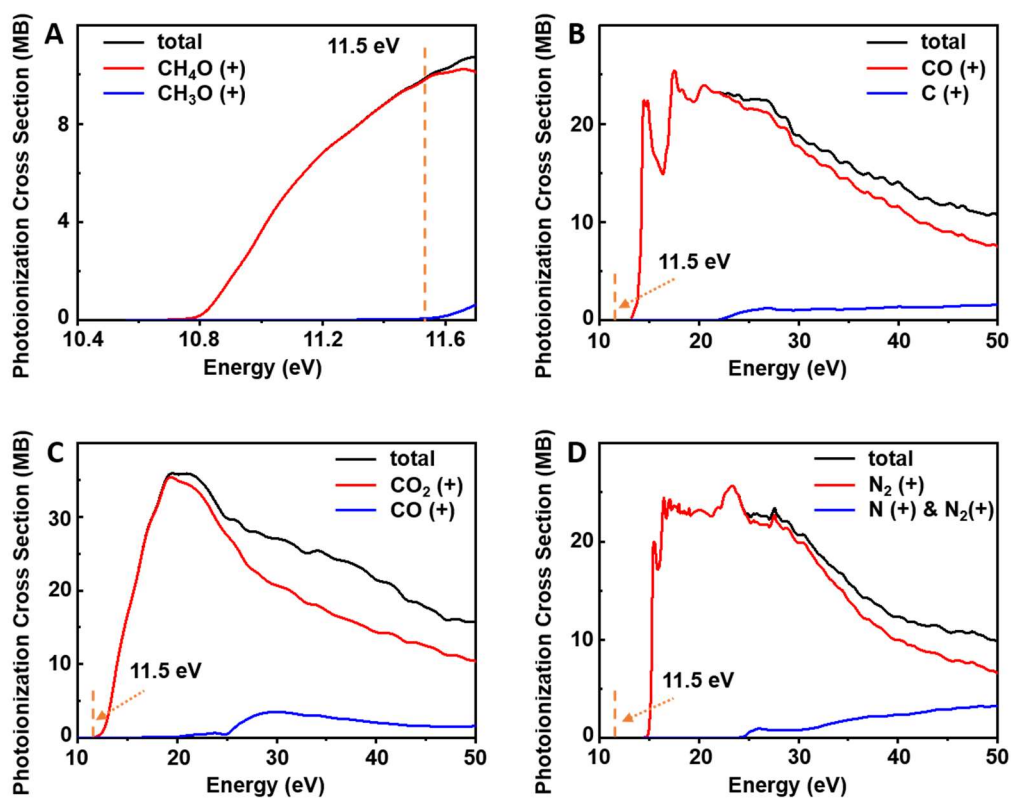


Figure S6. Synchrotron-based vacuum ultraviolet photoionization mass spectrometry (SVUV-PIMS). <http://flame.nslr.ustc.edu.cn/database/data.php>. Absolute photoionization cross sections for (a) CH₃OH, (b) CO, (c) CO₂, and (d) N₂.

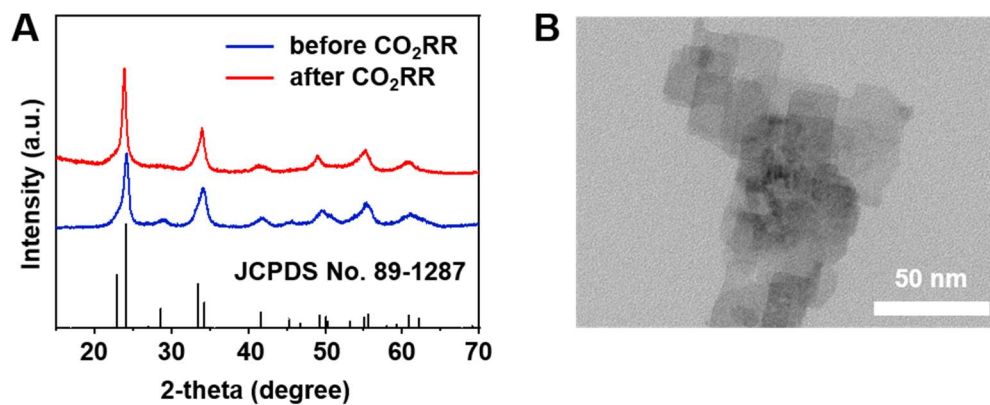


Figure S7. (A) XRD patterns of the Ti-WO₃ nanosheets before and after CO₂RR. (B) TEM image of the Ti-WO₃ nanosheets after CO₂RR.

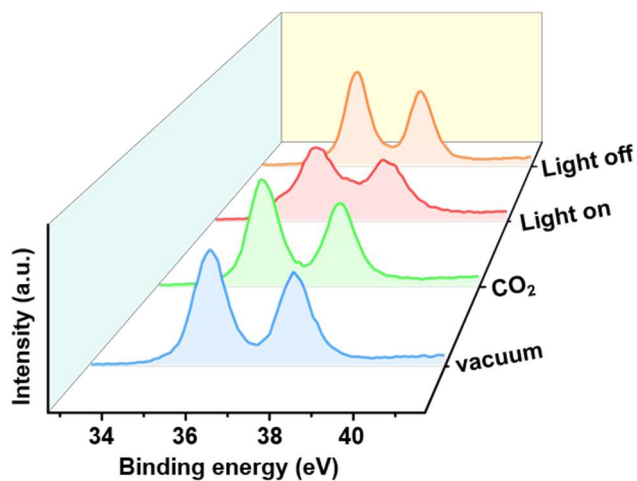


Figure S8. Quasi *in situ* XPS spectra of the WO₃ nanosheets during the CO₂ photoreduction.

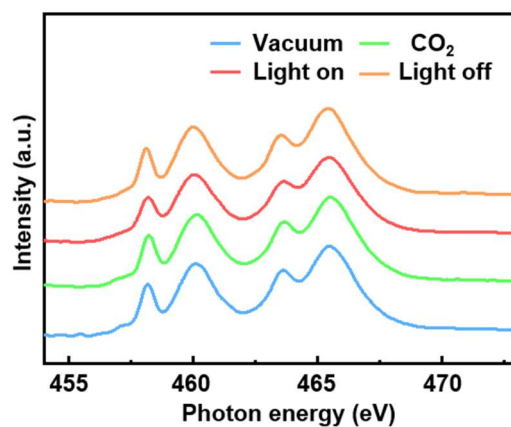


Figure S9. Quasi *in situ* XANES spectra of the Ti-WO₃ nanosheets during the CO₂ photoreduction.

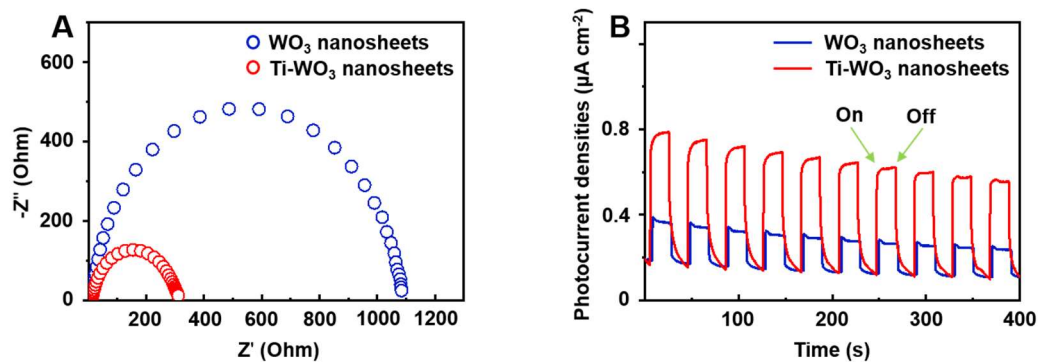


Figure S10. (A) Impedance test results of the Ti-WO₃ nanosheets and WO₃ nanosheets. (B) Transient photocurrent response of the Ti-WO₃ nanosheets and WO₃ nanosheets.

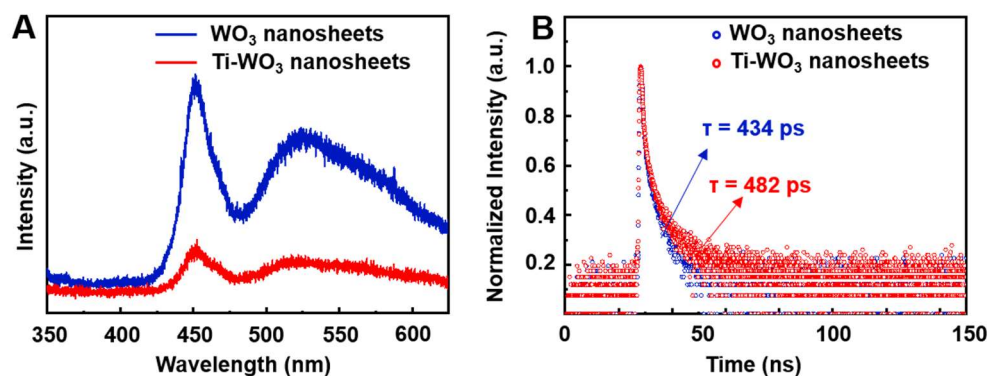


Figure S11. (A) Photoluminescence spectra of the Ti-WO₃ nanosheets and the WO₃ nanosheets under the excitation of 325 nm. (B) Time-resolved photoluminescence spectra of the Ti-WO₃ nanosheets and the Ti-WO₃ nanosheets.

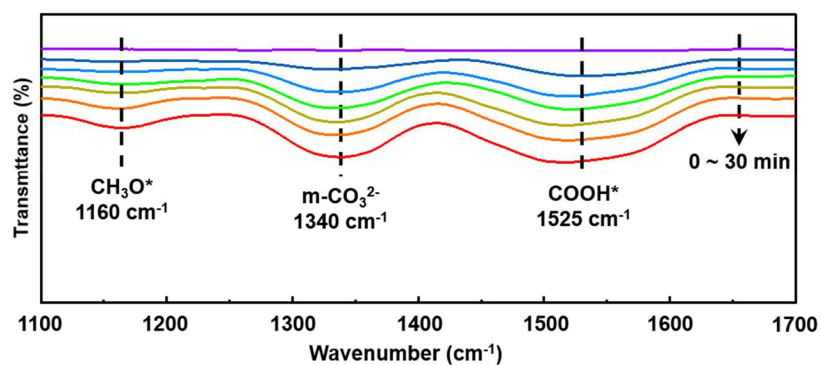


Figure S12. *In situ* FTIR spectra of the WO₃ nanosheets.

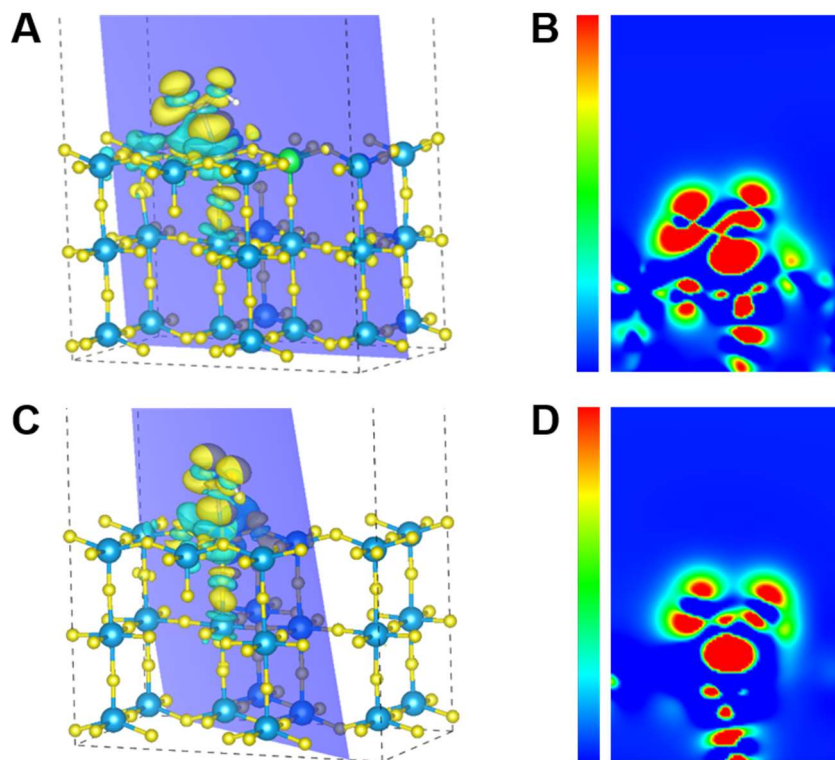


Figure S13. The difference density of electron distribution for COOH* intermediate over the Ti-WO₃ ultrathin layer slab (A-B) and the WO₃ ultrathin layer slab (C-D). The yellow and green isosurfaces correspond to the increase in the number of electrons and the depletion zone, respectively. The isosurfaces are 0.003 eÅ⁻³.

Table S1. Table of the electronic band structures for the Ti-WO₃ nanosheets and the WO₃ nanosheets (vs. NHE at pH = 7).

Sample	VBM (eV)	Bandgap (eV)	CBM (eV)
WO ₃ nanosheets	2.10	2.66	-0.56
Ti-WO ₃ nanosheets	1.66	2.59	-0.93

Table S2. Total energy (eV) of the reaction intermediates over the Ti-WO₃ ultrathin layer slab and the WO₃ ultrathin layer slab.

Sample	E _{DFT} (*)	E _{DFT} (COOH*)	E _{DFT} (CO*)	E _{DFT} (CHO*)	E _{DFT} (CH ₂ O*)	E _{DFT} (CH ₃ O*)	E _{DFT} (CH ₃ OH*)
WO ₃	-803.7	-829.47	-819.05	-823.07	-826.5	-831.25	-834.89
Ti/WO ₃	-801.75	-827.74	-816.88	-820.96	-824.38	-829.00	-832.52

Table S3. Free energy (eV) correction for species over the Ti-WO₃ ultrathin layer slab and the WO₃ ultrathin layer slab.

Species	E_{DFT}	E_{ZPE}	$T\Delta S$
H_2O	-14.21	0.56	0.67
H_2	-6.76	0.27	0.40
CO_2	-22.98	0.31	0.66
CH_3OH	-30.21	1.35	0.74
COOH^*	/	0.60	0.24
CO^*	/	0.15	0.26
CHO^*	/	0.42	0.17
CH_2O^*	/	0.74	0.17
CH_3O^*	/	1.04	0.25
CH_3OH^*	/	1.41	0.18

Table S4. Free energy (eV) of CO_2 electroreduction over the Ti- WO_3 ultrathin layer slab and the WO_3 ultrathin layer slab.

Sample	ΔG (*+ CO_2)	ΔG (COOH^*)	ΔG (CO^*)	ΔG (CHO^*)	ΔG (CH_2O^*)	ΔG (CH_3O^*)	ΔG (CH_3OH^*)	ΔG (*+ CH_3OH)
WO_3	0	1.37	0.44	0.23	0.56	-0.53	-0.28	0.08
Ti/ WO_3	0	1.15	0.66	0.39	0.73	-0.23	0.14	0.08

References

1. G. Kresse and J. Furthmüller, *Comput. Mater. Sci.*, 1996, **6**, 15-50.
2. D. K. Zhong and D. R. Gamelin, *J. Am. Chem. Soc.*, 2010, **132**, 4202-4207.
3. J. P. Perdew, K. Burke and M. Ernzerhof, *Phys. Rev. Lett.*, 1996, **77**, 3865-3868.
4. A. A. Peterson, F. Abild-Pedersen, F. Studt, J. Rossmeisl and J. K. Nørskov, *Energy Environ. Sci.*, 2010, **3**, 1311-1315.